Acoustic Emission and Modal Frequency Variation in Concrete Specimens under Four-Point Bending

applied sciences

MDPI

Article

Acoustic Emission and Modal Frequency Variation in Concrete Specimens under Four-Point Bending

Giuseppe Lacidogna *, Gianfranco Piana and Alberto Carpinteri

Department of Structural, Geotechnical and Building Engineering, Politecnico di Torino, Torino 10129, Italy; gianfranco.piana@polito.it (G.P.); alberto.carpinteri@polito.it (A.C.)

* Correspondence: giuseppe.lacidogna@polito.it; Tel.: +39-011-090-4871

Academic Editor: Dimitrios G. Aggelis

Received: 23 January 2017; Accepted: 22 March 2017; Published: 30 March 2017

Abstract: The Acoustic Emission (AE) and Dynamic Identification (DI) techniques were applied simultaneously, in an original way, to examine the stress dependent damage progress in pre-notched concrete beams tested in four-point bending. The damage mechanisms were characterized by analyzing the AE signals registered during the tests, conducted by increasing the specimen's vertical deflection. In particular, the dominant fracture mode was identified, and correlations between dissipated and emitted energies were investigated. Moreover, variations in the natural bending frequencies, produced by the crack advancement under loading, were detected and put in relation with the cumulated AE energy. Two different types of piezoelectric (PZT) sensors, operating in well distinct frequency ranges, were used to measure AE and modal signals. This study may be of interest with an outlook on possible correlations between a multi-parameter structural monitoring and the solution of inverse problems by numerical models.

Keywords: acoustic emission; natural frequency; material damage; concrete specimen; four-point bending test; brittle failure; softening; emitted energy; dissipated energy; PZT sensor

1. Introduction

The Acoustic Emission (AE) technique is currently used to investigate the damage evolution in ductile or brittle materials before the final failure [1,2]. The spatio-temporal evolution of ultrasonic AE signals is a direct result of cracking bonds during the fracture of materials. For this reason, this non-destructive monitoring method is useful for studying critical phenomena and to predict the durability and remaining life-time in laboratory and full-scale structures [3,4].

At the same time, low frequency Dynamic Identification (DI) techniques are currently used to extract modal parameters starting from time measures of displacements (or strains), velocities or accelerations. Non-destructive dynamic testing of structures allows information to be obtained about stability [5] and/or damage level and location [6]. Indeed, it is known that variations in structural stiffness are revealed by variations in modal parameters (primarily, frequencies and curvatures/shapes).

Today, both AE and DI techniques are thus used independently for damage identification and survey. The basic idea behind the present investigation is to combine both these techniques, therefore taking the advantages of a multi-parameter monitoring based on two independent methods. This could be of great interest for the structural health monitoring of large buildings and structures: AE signals can effectively be used as damage precursors and localizers, while experimental modal data can more conveniently be adopted to obtain information on the global stiffness and damage severity (e.g., crack depth) via inverse procedures based, for example, on finite element models. However, this study focuses on a single structural element as a first application. The benchmark is a concrete beam tested in the lab. To the best of the authors' knowledge, there are few studies in the literature where AE signals,

registered during the damage evolution in cracking beams, are put into relation with variations of global dynamic characteristics.

In this paper, the AE and DI techniques are applied to examine the stress dependent damage progress during four-point bending tests on pre-notched concrete beams. The damage mechanisms were characterized considering the AE signals obtained during the tests by increasing the vertical deflection of the sample. In particular, the dominant fracture mode was identified, and the correlations between dissipated and emitted energies were investigated [7]. Moreover, the variations of the first three natural bending frequencies, produced by the crack advancement under loading, were detected and correlated with the cumulated AE energy.

The tests were conducted using an MTS machine, operating in displacement-controlled conditions up to complete failure. The AE signals were acquired by piezoelectric transducers, sensitive in the frequency range from 80 to 400 kHz, attached near the notch. The natural frequencies were detected by piezoelectric pickups (PZT buzzers), sensitive in the range 0–20 kHz, placed along the beam surface. These sensors, typical of music technology, were recently applied to modal testing by some of the authors and found to be effective and robust in extracting natural frequencies and mode curvatures/shapes of straight and curved beams [8–10]. Their main advantages are high accuracy, small dimensions, low weight, easy usage, and low cost; they proved to have the same reliability of common laser sensors (but offering a much wider operating frequency range at a very low cost) and of piezoelectric accelerometers. They can also be conveniently coupled to audio acquisition devices without requiring calibration and filtering [8,9]. PZT buzzers were thus adopted in this work aiming at (i) testing their possible use on concrete specimens (so far they were only tested on metallic elements) and (ii) taking advantage of an existing experimental apparatus and the relevant know-how.

2. Acoustic Emission Monitoring

2.1. Critical Conditions and Fracture Modes

According to the AE technique, it is possible to detect the transient elastic waves related to each stress-induced crack propagation event inside a material. These waves can be captured and recorded by transducers applied on the surface of specimens or structural elements. The transducers are piezoelectric sensors that transform the energy of the elastic waves into electric signals. A suitable analysis of the AE waveform parameters (peak amplitude, duration time, and frequency) obtains detailed information about the damage evolution, such as the cracking pattern, the released energy, the prevalent fracture mode, and the achievement of critical conditions that anticipate the collapse. The last analysis can be performed by calculating the *b*-value from the Gutenberg-Richter (GR) law. Even though two different dimensional scales are involved, the GR law can be applied in the same way for earthquake distributions in seismic areas as well as for the structural monitoring by the AE technique [4,11,12].

The connection between fracture mode and recorded waves depends on different factors like geometric conditions, relative orientations, and propagation distances [13]. The identification of the cracking mode may be done with the AE wave's Rise Time (RT) (i.e., the time interval between the wave onset and its maximum amplitude), the value of the peak amplitude A, and the Average Frequency (AF). The ratio between the rise time (expressed in ms) and the peak amplitude (expressed in V) defines the Rise Angle (RA), as shown in Figure 1 [14–16]. The peak amplitude can be expressed in dB by the equation

$$A[\mathrm{dB}] = 20 \cdot \mathrm{Log}_{10}\left(\frac{V}{V_0}\right) \quad (1)$$

where V is the amplitude of the signal, and V_0 is the maximum amplitude of the background noise.

The AF (measured in Hz) is obtained from the AE ring-down count divided by the duration time of the signal. The AE ring-down count corresponds to the number of threshold crossings within the signal duration time [14–16].

The fracture mode is then characterized by the shape of the AE waveforms; low RAs and high AFs are typical for tensile crack propagations (Mode I, opening), whereas shear events (Mode II, sliding), usually generate longer waveforms, with higher RAs and lower AFs, as shown in Figure 1 [17–20]. Variations in the RA and AF values during the loading process identify a change in the prevalent failure mode of the specimen.

In general, a decrease in frequency might also be caused by the formation of large cracks during both tensile and shearing processes. In fact, it is reasonable to assume that high frequency waves are generated from small discontinuities that characterize the beginning of the damage process, whereas the low frequency ones can be produced from large cracks that usually develop during the final collapse [21].

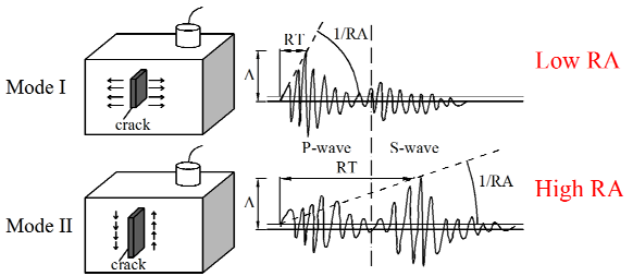

Figure 1. Typical waveforms for tensile and shear events. *A* is the amplitude and RT is the rise time (time between the onset and the point of maximum amplitude) of the waveforms. Reproduced with permission from [7], Elsevier, 2016.

2.2. Dissipated and Emitted Energies

Another interesting feature of the AE signals is that they can give insights into the process of energy dissipation and emission during the loading process. In this context, experimental analyses have evidenced that the scaling of the cumulative number of AE events by varying the specimen dimension can profitably be used to determine the physical dimension of the damage domain in disordered materials. In fact, the total number of AE events at the end of the test varies with the specimen size according to a power-law having a noninteger exponent that is directly related to the fractal character of the damage domain [3,22]. Alternatively, the characterization of the damage domain can also be obtained by means of a statistical analysis of the distribution of AE events in a single test [22]. From the viewpoint of energy dissipation and emission, the cumulative number of AE events and the energy content of the AE events are usually correlated to the mechanical energy dissipated during the complete failure process: namely, fracture energy in tension and crushing energy in compression [23,24].

However, recent studies carried out by Carpinteri and co-workers focusing on the catastrophic failure of rock specimens in compression have suggested that such a correlation is not always correct [25]. In particular, it was evidenced that a large amount of AE activity takes place during the post-peak snap-back instability. The typical shape of the load vs. displacement curve, when the global unstable behavior is fully captured—e.g., by controlling the compression test by means of the circumferential expansion instead of the longitudinal deformation—is that shown in Figure 2a. However, this very brittle mechanical response can also be observed under tension and bending loading conditions when brittle materials are tested in large and/or slender specimens. The behavior shown in Figure 2a is consequent to the fact that the energy dissipated through material damage is less than the elastic energy stored in the body. In this case, the portion of energy that is not dissipated by material damage (area *E* in Figure 2a) is abruptly emitted producing mechanical vibrations with propagation of elastic waves.

From the diagram in Figure 2a, therefore, three different energy components can be distinguished: the energy dissipated by material damage (gray area *D*), the surplus of elastic energy with respect

to the dissipated one (red-dashed area *E*), and the total released energy *R*, which is the sum of the two previous areas. When a catastrophic failure occurs, the AE energy seems to be correlated with the surplus of elastic energy [25]. Accordingly, such an energy component can be referred to as the emitted energy.

Certainly, global snap-back instabilities take place only under specific conditions (large sizes and slendernesses, and/or brittle materials), whereas in most cases a more stable response, represented by a softening behavior, is obtained. However, even in such cases, local discontinuities —which are an indication of snap-back or snap-through instabilities—are usually noticed in heterogeneous materials such as aggregative and fiber-reinforced materials. Such local phenomena evident at a microscale level are due to the fact that cracks grow in a discontinuous manner, with sudden propagations and arrests due to the bridging action of the secondary phases as well as by the rise and coalescence of microcracks in the process zone [26,27]. A load–displacement curve representative of a global softening behavior perturbed by multiple local instabilities is shown in Figure 2b. Each drop in the load carrying capacity occurring in the post-peak phase is related to a sudden crack propagation due, for instance, to the rupture of a reinforcing fiber. Then, the load carrying capacity is partially recovered following a path with a reduced stiffness. From the energetic point of view, each local instability is due to the emission of a surplus of elastic energy, which is not dissipated by the material damage (dashed areas in Figure 2b). This emitted energy can be detected by the AE sensors and can be used as a damage indicator.

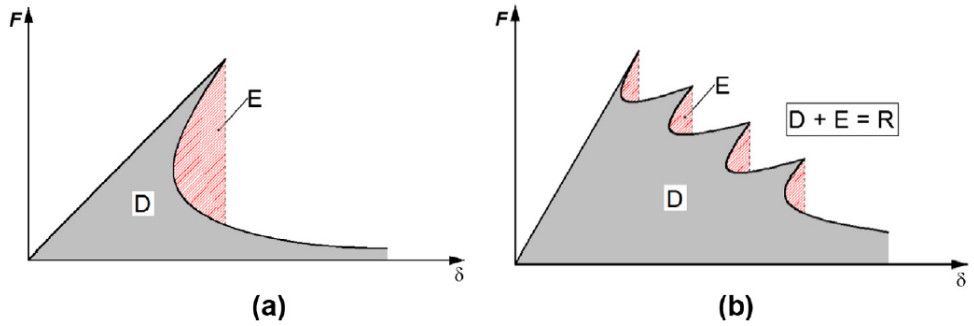

Figure 2. Load–displacement curves representing (**a**) a catastrophic failure (single snap-back) and (**b**) a global softening behavior perturbed by multiple local instabilities (snap-backs). The grey areas identify the dissipated energy, *D*, whereas the red (dashed) ones represent the emitted energy, *E*. The total released energy, *R*, is the summation of the two previous areas: $D + E = R$. Reproduced with permission from [7], Elsevier, 2016.

2.3. Results from Previous TPB Tests and Aim of Present Study

In a recent paper [7], the AE parameters acquired during three-point bending (TPB) tests on notched concrete beams and a compression test on a cylindrical specimen were analyzed. These analyses were performed in order to identify the dominant fracture mode and to investigate the evolution of the released, dissipated, and emitted energies during the test and their mutual correlations. While the dissipated energy was determined directly from the experimental load–displacement curves, the emitted energy was obtained from the AE signals energy detected by the sensors. The proposed comparisons between the dissipated and emitted energies for three different specimen sizes—carried out both in terms of their cumulative values at the end of the tests and of the evolution of their rates during the loading process—suggest that there is no direct proportionality between them. In particular, a considerable increase in the fracture energy was evidenced by increasing the specimen size, whereas an opposite trend was obtained for the AE energy per unit surface [7]. According to the interpretation proposed in [25], the AE energy should be correlated to the surplus of elastic energy with respect to the dissipated one that is emitted in correspondence of unstable behaviors.

The aim of the present study is to survey the damage process in notched concrete specimens by analyzing both the AE signals and the modal frequency variations. The specimens have the same

geometry and material properties as one of the beams considered in [7]. Here, they were tested in a four-point bending configuration instead of a three-point one. The former configuration, compared to the three-point bending scheme, may result in a more brittle behavior of the specimen, with unstable crack growth [28]. However, the four-point configuration is more suitable for the dynamic testing of a specimen notched at midlength; in fact, this avoids having a support—and therefore a fixed node in the modal shapes—in correspondence to the weakened section. As it is well known from structural dynamics, a decrease in the structural stiffness will result in decreased frequencies [29,30]. Therefore, extracting the natural frequencies under loading can directly give information about the reduction in the beam global stiffness produced by crack development and propagation; this may be indirectly brought back to the crack advancement by means, for example, of numerical models [31–34]. In the case under investigation, cracks would preferably develop near the notch. More in general, provided a sufficient number of AE sensors is mounted (the number adopted here was insufficient), AE signal analysis could allow for localizing cracks. Moreover, in a case such as the one under investigation, localization of AE sources could also allow for more information about the crack advancement. However, in complex full-scale structures (bridges, dams, buildings, etc.), localization of cracks is not straightforward due to strong signal attenuation (especially for the higher frequencies), which would require a great number of sensors to detect each cracking event. Therefore, specific information about crack advancement are rather difficult to obtain from AE. On the other hand, information on the crack propagation may be obtained by analyzing modal parameters, especially if the damage location is known. Therefore, it results that combining AE and DI techniques may be of interest in the monitoring of large structures. To sum up, the prime objective of the this study was to monitor the same damage process by two independent techniques, while at the same time understanding possible relations between the two sets of data. Linear finite element models helped in getting a first evaluation of the crack propagation via modal analysis.

3. Experimental Tests

3.1. Specimen Characteristics

Three equal concrete beams were tested. The beams, having a square cross-section, were pre-notched at midlength for one half of the depth and for the entire width. The specimens' geometry and the loading configuration are shown in Figure 3. The geometric characteristics are listed in Table 1, whereas the mechanical properties are reported in Table 2. The mass density ρ and characteristic compression strength R_{ck} were obtained by averaging the values of laboratory tests made on five cubic specimens of side 160 mm. The value of the fracture energy G_f was taken from [7]. All the remaining properties in Table 2 were evaluated according to the Italian technical regulations [35], starting from the measured compression strength.

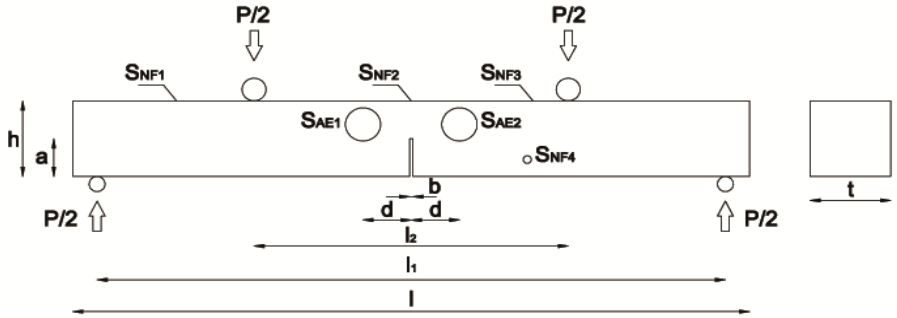

Figure 3. Specimen geometry and loading configuration. S_{AE1} and S_{AE2} are the sensors adopted to detect the AE signals, while S_{NF1}–S_{NF4} are the sensors used to reveal the natural frequencies.

Table 1. Geometric dimensions of specimens (in mm).

l	h	t	a	b	l_1	l_2	d
840	100	100	50	4	780	390	60

Table 2. Mechanical properties of specimens.

Mass Density ρ (kg/m^3)	Cubic Compression Strength R_{ck} (MPa)	Cylindrical Compression Strength f_{ck} (MPa)	Average Bending Strength f_{cfm} (MPa)	Average Tensile Strength f_{ctm} (MPa)	Average Young's Modulus E_{cm} (MPa)	Fracture Energy G_f (N/m)
2,310	26.4	21.9	2.8	2.4	30,570	118

3.2. Experimental Set-Up and Testing Procedures

The experimental set-up is shown in Figures 3 and 4. The tests were conducted using a servo-hydraulic MTS testing machine. The samples were tested up to final failure by increasing the vertical displacement δ of the hydraulic jack with a velocity of 1 μm/s. Moreover, the crack mouth opening displacement (CMOD) was also measured.

The specimen was equipped with four piezoelectric pickups (piezo-ceramic buzzers) and two piezoelectric AE detectors, positioned as shown in Figure 3. The former (S_{NF1}–S_{NF4} in Figure 3) were used to evaluate the element natural frequencies for increasing loads and during crack propagation. The adopted sensors are the JPR Plustone 400-403 disks, whose main characteristics are external diameter 20 mm, frequency range 0 to 20 kHz, resonant frequency 6.0 ± 0.5 kHz, operating temperature −20 to +50 °C, and weight ~1 g. The data were collected by an 8-channel Audiobox 1818VS1 acquisition device by PreSonus (Baton Rouge, LA, USA); the sampling frequency was set equal to 48 kHz.

The piezoelectric transducers S_{AE1} and S_{AE2} in Figure 3 (active element: ceramics, case material: anodized aluminum, case shape: circular $d \times h = 50 \times 35$ mm, weight: 110 g), produced by Leane Net S.r.l. (Sarzana, Italy), detected the AE signals. The former was a wideband sensor (bandwidth 80–400 kHz), while the latter was a resonant one (resonance frequency 160 kHz). The connection between sensors and acquisition device was realized by coaxial cables (BNC female) to reduce the effects of electromagnetic noise. The data were acquired by an 8-channel national instruments digitizer, setting the acquisition threshold to 5 mV and adopting a sampling frequency of 1 Msample/s. The registered signals were first amplified up to 40 dB and then processed.

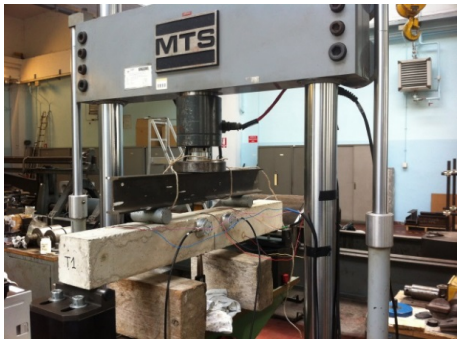

Figure 4. Experimental set-up of the four-point bending test.

Two kinds of tests were conducted:

1. A test where the imposed displacement was monotonically and continuously increased up to the final failure of the specimen, during which the load–displacement curve was registered and AEs were detected;
2. Two tests where the imposed displacement was increased monotonically, but discontinuously, in several steps. At the end of each step of increment in displacement, the free response

signals provoked by an external impulsive force were acquired via the piezoelectric pickups to evaluate the natural frequencies. Moreover, the load–displacement curve and the AE signals were registered.

4. Results

Figure 5 shows the load–displacement curves obtained from the three tests. The load and displacement values reported in the figure are the force measured by the loading cell, and the displacement of the hydraulic jack, respectively. In particular, the load values do not include the weight of the concrete specimen, of the steel I beam and cylinders, or of transducers and cables (almost negligible), for a total of about 0.3 kN. Tests 1 and 2 were of the kind (b) described above, whereas test 3 was of the kind (a). As expected, the curve related to test 3 is more regular than those related to tests 1 and 2 that, conversely, reflect the discontinuous character of the loading process. In fact, not only was the test stopped several times, but the beam was also perturbed by external impulses at the end of each incremental step to excite the free vibrations. This explains the numerous jumps in the load–displacement curve of the first two tests. Moreover, the softening branch was globally quite stable for test 1, while an unstable crack propagation was registered for tests 2 and 3, where global snap-backs were observed (Figure 5).

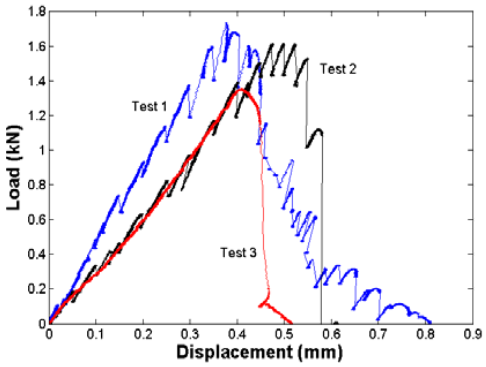

Figure 5. Experimental load vs. displacement curves for the three four-point bending tests conducted.

In Figure 6a, the load vs. displacement and cumulated AE energy vs. displacement diagrams of test 1 are superimposed. The figure shows that no sensible AE was detected until about the 90% of the peak load (however, first events were registered near the 60% of the peak load, see the zoom in the box of Figure 6a). A large jump in the AE energy appears in correspondence of the maximum load point after which the AE energy progressively increases up to the end of the test.

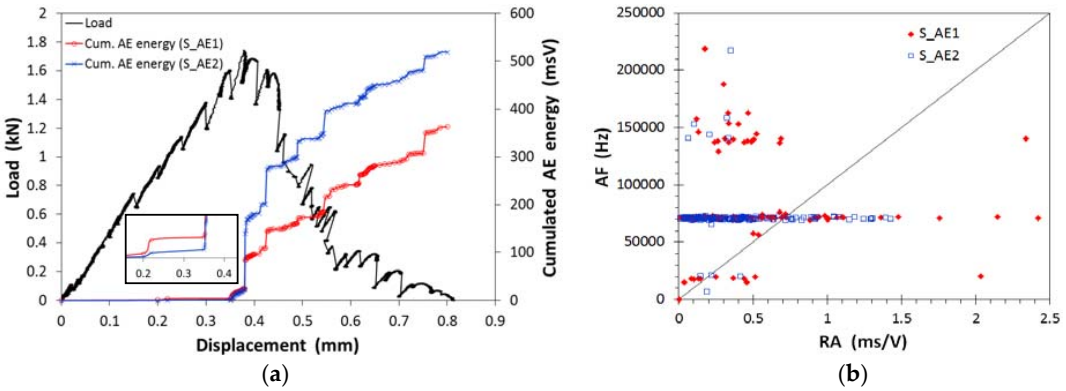

Figure 6. Test 1: (**a**) load and cumulated AE energy vs. displacement diagrams; (**b**) RA values of detected Acoustic Emission (AE) events (S_{AE1} = wideband sensor, S_{AE2} = resonant sensor).

The failure occurred due to crack propagation in the notched section, provoked principally by tensile stresses. Considering the static scheme, plus the small ratio self-weight/maximum external force applied and the stress diffusion according to Saint Venant's principle, the central part of the intermediate span was mainly subjected to bending stresses (see Figure 7a). A sub-vertical main crack developed near the notch: the initial inclined path was followed by an almost vertical propagation (Figure 7b). The fracture mode of test 1 was analyzed by means of the relationship between RA and AF values estimated for each sensor, as shown in Figure 6b. Considering that a decrease in the AFs by approaching the final stage of the test is obtained, and that the RA values are all lower than 2.5 ms/V, a dominant presence of tensile cracks (Mode I) characterizes the damage evolution up to the final collapse [7,13,16–18]. However, a certain amount of Mode II cracks also appeared due to local mixed mode crack propagations around inhomogeneities. These findings were in agreement with literature studies, e.g., see [36,37]. Direct visual observation (when possible) and identification of the cracking mode by AE wave's RT analysis, as far as not supported by other survey methods such as digital image correlation [38] or X-ray diffraction analysis [39], was important; in fact, this allowed for the characterizing the cracking mode based on information obtained from a small number of sensors.

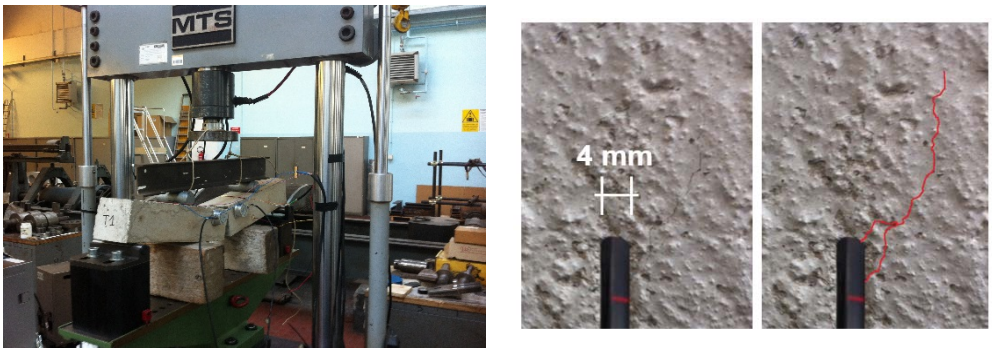

(**a**) (**b**)

Figure 7. Test 1: (**a**) collapsed specimen and (**b**) particular of the crack developed near the notch.

Figure 8a,b shows the load vs. displacement and cumulated AE energy vs. displacement curves of test 2, 3, respectively. As previously pointed out, the load–displacement graph of tests 2 and 3 denote a more brittle behavior than that of test 1 (see the large load jumps in the post-peak phase in Figure 8a,b). In order to describe this catastrophic behavior and the relevant acoustic emission better, the effect of the self-weights mentioned above is shown in Figure 8a,b (see negative load values), so that the entire load–displacement path can be visualized. As already pointed-out, the irregular (regular) shape of the loading curve of test 2 (3) is due to the discontinuous (continuous) character of the loading test. As regards to the acoustic emission, the cumulated AE energy graphs in Figure 8 show large jumps in correspondence to criticalities. In particular, Figure 8a (test 2) shows that AEs started near the peak load and afterward exhibited sharp increments near the global snap-backs and the final collapse. Figure 8b (test 3) shows first AEs near about the 90% of the peak load, followed by a large increment in correspondence to the peak load, just before the global snap-back, several increments in correspondence to local instabilities (say, local snap-backs), and a last sharp increment just before the final collapse.

Since the pickups captured frequencies corresponding to all possible motions of the beam in space, namely longitudinal, torsional, vertical and lateral bending, and combination of them, a preliminary modal analysis was run to identify the frequencies of interest. A 2-D finite element beam model was therefore implemented in LUSAS software using plane stress elements [40]. Figure 9a shows the first three numerical frequencies of vertical vibration obtained for the unloaded pre-notched beam (i.e., in the stress-free condition) resting on four supports.

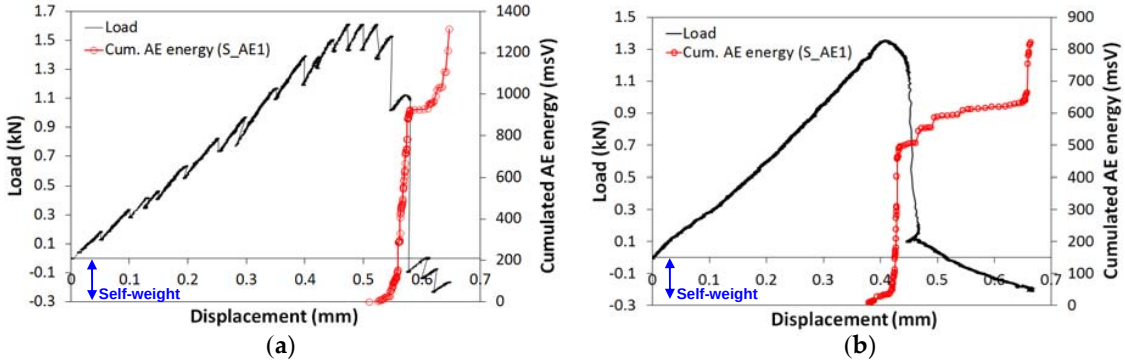

Figure 8. Load and cumulated AE energy vs. displacement diagrams for (**a**) test 2 and (**b**) test 3 (S_{AE1} = wideband sensor).

Figure 9b shows the variation of the first three natural frequencies with the imposed vertical displacement for test 1. The curves show that the eigenfrequencies remained constant during the loading phase almost until the peak load was reached (the corresponding displacement is equal to 0.38 mm; see Figure 5). After, they started decreasing progressively. In particular, the reduction was equal to about 28%, 18%, and 8% for the first, the second, and the third frequency, respectively. This reductions in frequency can be correlated to a decrement of the element stiffness and, therefore, to the crack advancement [41]. As one might have expected, higher frequencies are less influenced than lower ones; thus, in monitoring the damage evolution, experimental frequency identification can be limited to a few lower frequencies.

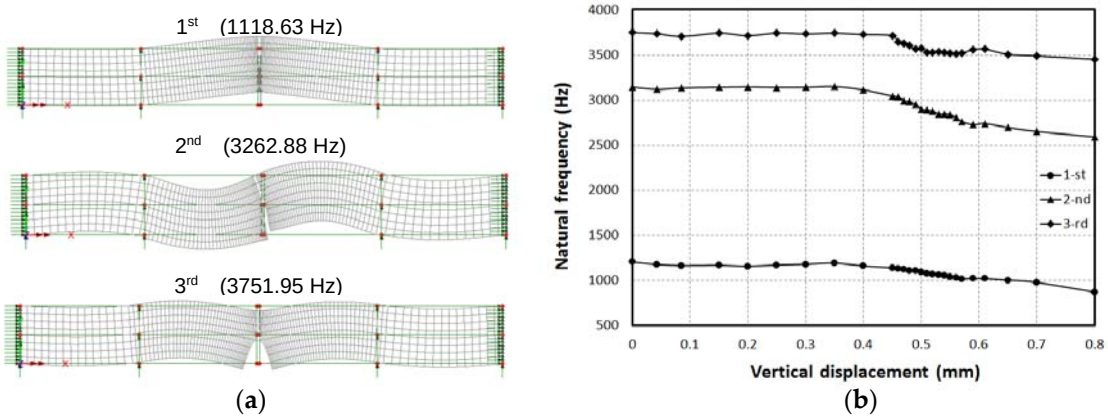

Figure 9. Test 1: (**a**) first three numerical (FEM) bending modes and related frequencies (unloaded beam, initial notch depth) and (**b**) experimental natural frequencies vs. displacement curves.

In Figure 10, a correlation between natural frequency variation and AEs is proposed. Figure 10a shows the first three experimental natural frequencies and the cumulated curve of AE energy vs. the vertical displacement. The diagrams clearly show that the natural frequencies decrease while the AE energy increases, i.e., as the damage advances. This also results clear from Figure 10b–d, where the first, second, and third natural frequencies of vertical vibration are plotted against the cumulated AE energy computed from the signals received by the AE sensors (S_{AE1} = wideband sensor, S_{AE2} = resonant sensor). In fact, the larger the amount of energy dissipated and emitted through material damage, the smaller the amount of elastic energy available to be converted into kinetic energy of vibration. The qualitative trends are similar for sensors S_{AE1} and S_{AE2}; the only difference is in the quantity of energy registered by the two sensors. It is interesting to note that the natural frequencies decrease discontinuously with the cumulated AE energy (AEs are discontinuous, see Figure 10a). In particular,

we observe that a certain amount of AE energy must be emitted before initial/new decreases in the natural frequencies can be observed (Figure 10b–d); however, such amount of energy is not a constant.

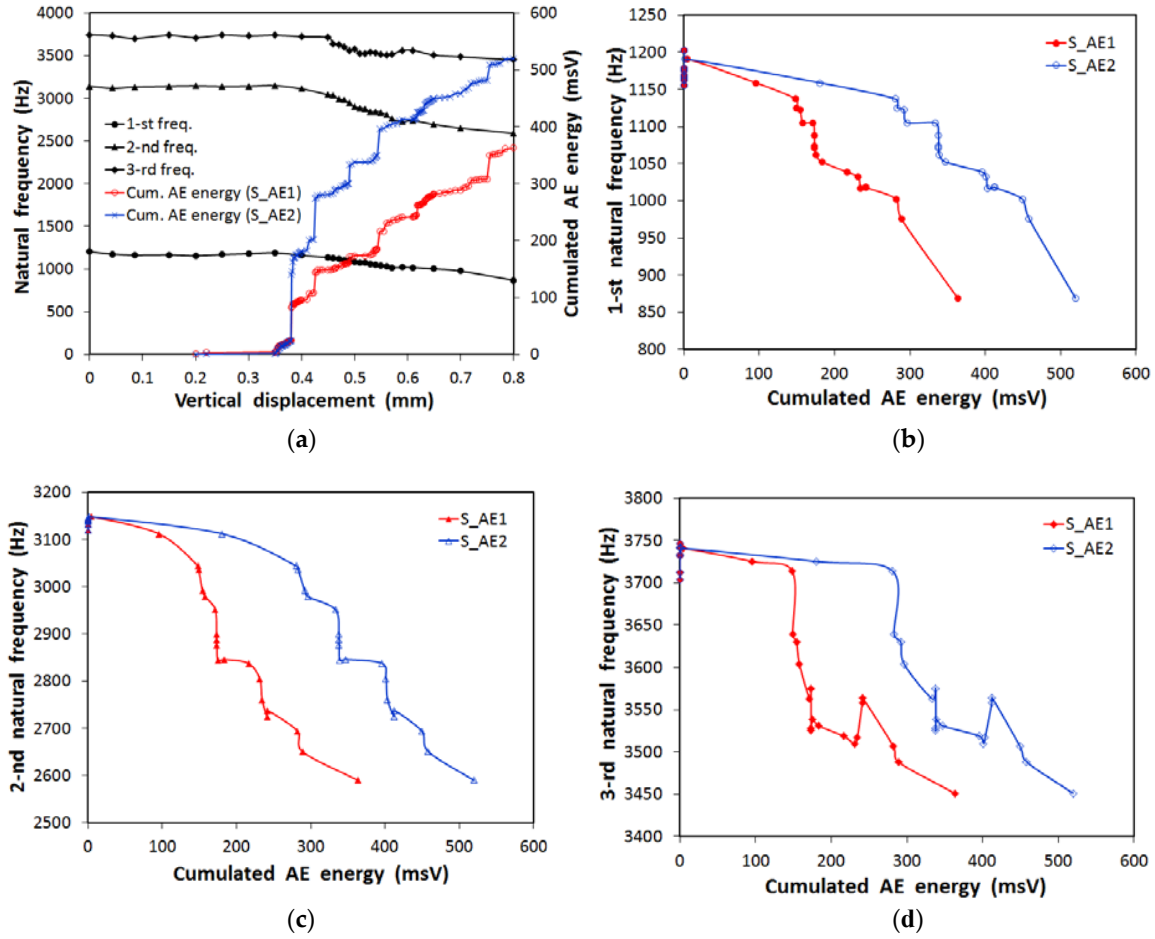

Figure 10. Test 1: (**a**) experimental natural frequencies and cumulated AE energy vs. vertical displacement; (**b**–**d**) first, second, third natural frequency vs. cumulated AE energy (S_{AE1} = wideband sensor, S_{AE2} = resonant sensor).

Finite element models of the unloaded pre-notched beam were used to look for a first estimate of the crack advancement by comparing measured and calculated frequencies. The notch depth was increased from the initial value till the 95% of the beam depth. The following values of the relative notch depth $\xi = a/h$ were considered: ξ = 0.5, 0.625, 0.75, 0.875, and 0.95. They correspond respectively to the following depth of the ligament, h–a: 5, 3.75, 2.5, 1.25, and 0.5 cm. The corresponding fundamental frequencies are respectively equal to the following approximate values: 1120, 985, 915, 885, and 875 Hz. Figure 11a shows the numerical fundamental vibration mode and frequency for the previous values of the relative notch depth ξ. Figure 11b proposes a comparison between the numerical values of the fundamental frequency and the parabolic approximation of the corresponding experimental values. Such a comparison represents a simple way to obtain a first evaluation of the crack advancement. At the same time, a more sophisticated analysis accounting for the nonlinear stress–strain relationship of concrete (both in tension and compression), together with the presence of the loadings (self-weight and external forces), would simulate better the experimental test, allowing for the study of linear vibrations at different loading levels. Further refinements could also be achieved by nonlinear modeling of breathing cracks [33,34,42]. However, the previous refinements are beyond the scope of the present study.

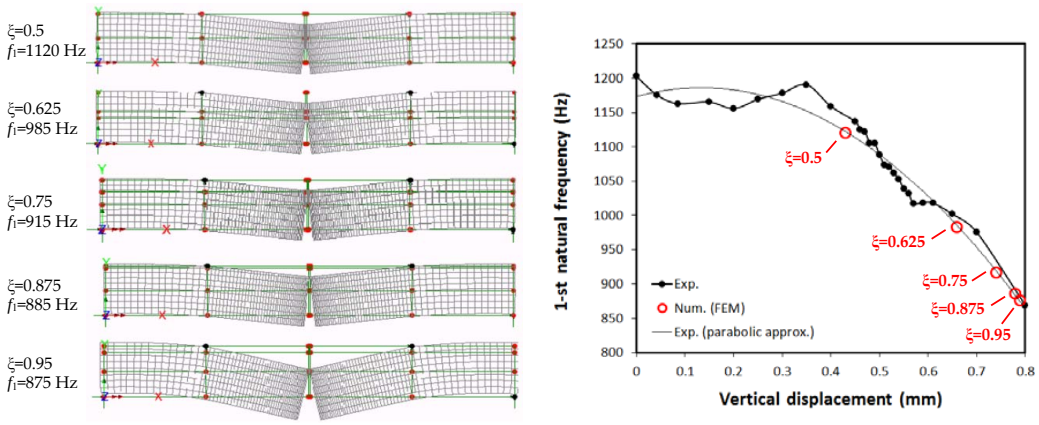

Figure 11. (**a**) Numerical (FEM) fundamental vibration mode and frequency of the unloaded beam for increasing notch depth ($\xi = a/h$) and (**b**) approximate evaluation of crack advancement based on measured and calculated (FEM) fundamental frequencies.

5. Discussion

The aim of the present study was to analyze both AE signals and modal frequency variations during the loading and damage of pre-notched concrete beams. The specimens were tested in the four-point bending configuration by an MTS universal machine. The tests were conducted by controlling the axial displacement of the hydraulic jack and continued up to complete failure. As a comment on the general trend of the conducted tests, the load–displacement curves revealed an elasto-softening behavior of the specimens, with multiple snap-back instabilities in the post-peak branch. In two cases, a globally unstable behavior was registered in the softening branch; this character is reflected by the acoustic emission energy analysis. We also remark that piezoelectric pickups typical of music technology, recently adopted by some of the authors to extract modal parameters of slender metallic elements in the lab [8–10], were successfully used here, as long as the natural frequencies of stubby concrete specimens are extracted. The main remarks, related to the results of the present study, can be summarized as follows.

AE energy and natural bending frequencies were used as two independent parameters to monitor the same damage process. It was found that the natural bending frequencies decrease as the cumulated AE energy increases. In fact, both these kinds of parameters can be used as damage indicators: the former is correlated to the energy emitted by the material during crack formation and propagation, while the latter is correlated to the loss in global stiffness due to the cross-section reduction provoked by crack propagation. First acoustic emissions were registered even before the peak load, while no sensible variations in the natural frequencies were observed. After the peak load, as was expected, AEs increased up to final failure, while the natural frequencies progressively decreased as the vertical displacement was increased. The obtained trends suggest that a certain amount of AE energy (which, however, is not a constant) must be emitted by the specimen before initial/new decreases in the natural frequencies can be observed. Lastly, linear finite element models of the unloaded specimen, where the notch depth was varied, were used to look for a first correlation between the frequency reduction and the crack propagation (simplifying the actual phenomenon). Such a correlation is of interest to acquire information about the cross-section integrity, and therefore to evaluate its resisting capacity. However, the former issue was addressed here only partially (a deeper investigation would have required performing more sophisticated nonlinear analyses), whereas the latter was not addressed at all, it being beyond the scope of the present study. On the other hand, much literature on the evaluation of crack location and depth based on measured natural frequencies (and modes) exists (e.g., see [43–52]).

This work represents a first attempt to correlate AE signals produced by material damage with variations in the natural vibration frequencies of a cracking element. Such a combination between the AE and the DI techniques could have significant implications in structural monitoring. More precisely, the AE signal analysis can effectively be used as damage precursor, detector, and identifier; the analysis of the variation in modal properties can more conveniently be adopted to catch information about the global rigidity of the structure and, eventually, to evaluate its damage level and safety by inverse procedures. The main steps of a possible combined monitoring of a complex structure can be resumed as follows:

1. AE and DI sensors should be installed on the structure to be monitored (both monitoring systems should be completed with the relevant instrumentation);
2. Recorded AE signals should be analyzed in order to reveal and, possibly, localize and/or characterize damage;
3. The most relevant natural frequencies (and, possibly, curvature/modes) should be identified regularly, especially when AE is higher. Sensible variations (not related, for example, to thermal or loading cycles) in modal parameters with respect to the corresponding quantities of the integer structure (e.g., monotonic frequency reductions, localizations in modal curvatures, etc.) should be carefully evaluated;
4. Numerical (e.g., FEM) models of the damaged structure should be implemented and the relevant inverse dynamic problem solved to investigate the damage level. For example, localized damage sources (e.g., cross-sections reductions simulating cracks) should be inserted and their severity arranged (e.g., the crack depth varied) until a good match between numerical and experimental parameters (e.g., the frequencies) is reached. This could provide an estimate of the crack depth;
5. Based on the results of both the AE analysis in Step 2 and the dynamic simulations in Step 4, the resisting capacity and/or the safety of the structure could be evaluated according to pre-defined criteria (Design Standards, Recommendations, etc.).

The above procedure may increase the reliability in structural monitoring of full-scale structures (the two experimental techniques are independent) by combining the advantages of (i) damage precursor data provided by the AE technique, (ii) damage location based on measured AE and modal data, and (iii) direct information about the global structural stiffness, that can be correlated by numerical models tuned on measured modal characteristics to damage level and resisting capacity (information not easy to obtain for a large structure via AE monitoring).

In conclusion, the main benefit of the present study is the combination of two independent techniques for the analysis of the damage progress of a structural element. Thus, this work may be useful with an outlook to multi-parameter damage identification and monitoring.

Acknowledgments: The authors gratefully acknowledge Eng. C. Della Rocca for his helpful contribution in the acquisition and analysis of experimental data.

Author Contributions: G.L. and G.P. conceived and performed the experiments, and wrote the paper, giving main contributions on acoustic emission and modal analysis, respectively. A.C. supervised the research.

Conflicts of Interest: The authors declare no conflict of interest.

References

1. Ohtsu, M. The history and development of acoustic emission in concrete engineering. *Mag. Concr. Res.* **1996**, *48*, 321–330. [CrossRef]
2. Grosse, C.; Ohtsu, M. (Eds.) *Acoustic Emission Testing*; Springer: Berlin, Germany, 2008.
3. Carpinteri, A.; Lacidogna, G.; Pugno, N. Structural damage diagnosis and life-time assessment by acoustic emission monitoring. *Eng. Fract. Mech.* **2007**, *74*, 273–289. [CrossRef]
4. Carpinteri, A.; Lacidogna, G.; Puzzi, S. From criticality to final collapse: Evolution of the *b*-value from 1.5 to 1.0. *Chaos Soliton Fract.* **2009**, *41*, 843–853. [CrossRef]

5. Carpinteri, A.; Malvano, R.; Manuello, A.; Piana, G. Fundamental frequency evolution in slender beams subjected to imposed axial displacements. *J. Sound. Vib.* **2014**, *333*, 2390–2403. [CrossRef]
6. Dessi, D.; Camerlengo, G. Damage identification techniques via modal curvature analysis: Overview and comparison. *Mech. Syst. Signal Process.* **2015**, *52–53*, 181–205. [CrossRef]
7. Carpinteri, A.; Lacidogna, G.; Corrado, M.; Di Battista, E. Cracking and crackling in concrete-like materials: A dynamic energy balance. *Eng. Fract. Mech.* **2016**, *155*, 130–144. [CrossRef]
8. Piana, G.; Lofrano, E.; Carpinteri, A.; Paolone, A.; Ruta, G. Experimental modal analysis of straight and curved slender beams by piezoelectric transducers. *Meccanica* **2016**, *51*, 2797–2811. [CrossRef]
9. Piana, G.; Lofrano, E.; Manuello, A.; Ruta, G. Natural frequencies and buckling of compressed non-symmetric thin-walled beams. *Thin. Wall Struct.* **2017**, *111*, 189–196. [CrossRef]
10. Piana, G.; Lofrano, E.; Manuello, A.; Ruta, G.; Carpinteri, A. Compressive buckling for symmetric TWB with non-zero warping stiffness. *Eng. Struct.* **2017**, *135*, 246–258. [CrossRef]
11. Scholz, C.H. The frequency-magnitude relation of microfracturing in rock and its relation to earthquakes. *Bull. Seismol. Soc. Am.* **1968**, *58*, 399–415.
12. Carpinteri, A.; Lacidogna, G.; Niccolini, G.; Puzzi, S. Critical defect size distributions in concrete structures detected by the acoustic emission technique. *Meccanica* **2008**, *43*, 349–363. [CrossRef]
13. Aggelis, D.G.; Mpalaskas, A.C.; Ntalakas, D.; Matikas, T.E. Effect of wave distortion on acoustic emission characterization of cementitious materials. *Constr. Build. Mater.* **2012**, *35*, 183–190. [CrossRef]
14. Recommendation of RILEM TC 212-ACD. Acoustic emission and related NDE techniques for crack detection and damage evaluation in concrete: Measurement method for acoustic emission signals in concrete. *Mater. Struct.* **2010**, *43*, 1177–1181.
15. Recommendation of RILEM TC 212-ACD. Acoustic emission and related NDE techniques for crack detection and damage evaluation in concrete: Test method for damage qualification of reinforced concrete beams by acoustic emission. *Mater. Struct.* **2010**, *43*, 1183–1186.
16. Recommendation of RILEM TC 212-ACD. Acoustic emission and related NDE techniques for crack detection and damage evaluation in concrete: Test method for classification of active cracks in concrete by acoustic emission. *Mater. Struct.* **2010**, *43*, 1187–1189.
17. Soulioti, D.; Barkoula, N.M.; Paipetis, A.; Matikas, T.E.; Shiotani, T.; Aggelis, D.G. Acoustic emission behavior of steel fibre reinforced concrete under bending. *Constr. Build. Mater.* **2009**, *23*, 3532–3536. [CrossRef]
18. Ohno, K.; Ohtsu, M. Crack classification in concrete based on acoustic emission. *Constr. Build. Mater.* **2010**, *24*, 2339–2346. [CrossRef]
19. Aggelis, D.G. Classification of cracking mode in concrete by acoustic emission parameters. *Mech. Res. Commun.* **2011**, *38*, 153–157. [CrossRef]
20. Aldahdooh, M.A.A.; Bunnori, N.M. Crack classification in reinforced concrete beams with varying thicknesses by mean of acoustic emission signal features. *Constr. Build. Mater.* **2013**, *45*, 282–288. [CrossRef]
21. Landis, E.N.; Shah, S.P. Frequency-dependent stress wave attenuation in cement-based materials. *J. Eng. Mech. ASCE* **1995**, *121*, 737–743. [CrossRef]
22. Carpinteri, A.; Corrado, M.; Lacidogna, G. Three different approaches for damage domain characterization in disordered materials: Fractal energy density, *b*-value statistics, renormalization group theory. *Mech. Mater.* **2012**, *53*, 15–28. [CrossRef]
23. Muralidhara, S.; Raghu Prasad, B.K.; Eskandari, H.; Karihaloo, B.L. Fracture process zone size and true fracture energy of concrete using acoustic emission. *Constr. Build. Mater.* **2010**, *24*, 479–486. [CrossRef]
24. Landis, E.N.; Baillon, L. Experiments to relate acoustic emission energy to fracture energy of concrete. *J. Eng. Mech. ASCE* **2002**, *128*, 698–702. [CrossRef]
25. Carpinteri, A.; Corrado, M.; Lacidogna, G. Heterogeneous materials in compression: Correlations between absorbed, released and acoustic emission energies. *Eng. Fail. Anal.* **2013**, *33*, 236–250. [CrossRef]
26. Carpinteri, A.; Monetto, I. Snap-back analysis of fracture evolution in multi-cracked solids using boundary element method. *Int. J. Fract.* **1999**, *98*, 225–241. [CrossRef]
27. Carpinteri, A.; Massabò, R. Continuous vs discontinuous bridged-crack model for fiber-reinforced materials in flexure. *Int. J. Solids Struct.* **1997**, *34*, 2321–2338. [CrossRef]
28. Tandon, S.; Faber, K.T.; Bažant, Z.P. Crack stability in the fracture of cementitious materials. *Mater. Res. Soc. Symp. Proc.* **1995**, *370*, 387–396. [CrossRef]
29. Clough, R.W.; Penzien, J. *Dynamics of Structures*; McGraw-Hill: New York, NY, USA, 1975.

30. De Silva, C.W. *Vibration: Fundamentals and Practice*; CRC Press: Boca Raton, FL, USA, 2000.
31. Liang, R.Y.; Hu, J.; Choy, F. Theoretical study of crack-induced eigenfrequency changes on beam structures. *J. Eng. Mech.* **1992**, *118*, 384–396. [CrossRef]
32. Dimarogonas, A.D. Vibration of cracked structures: A state of the art review. *Eng. Fract. Mech.* **1996**, *55*, 931–857. [CrossRef]
33. Bouboulas, A.S.; Georgantzinos, S.K.; Anifantis, N.K. Vibration analysis of cracked beams using the finite element method. In *Advances in Vibration Engineering and Structural Dynamics*; Beltran-Carbajal, F., Ed.; InTech: Rijeka, Croatia, 2012; pp. 181–204.
34. Friswell, M.I.; Penny, J.E.T. Crack modeling for structural health monitoring. *Struct. Health Monit.* **2002**, *1*, 139–l48. [CrossRef]
35. D.M. 14/01/2008. Norme Tecniche per le Costruzioni. *Gazzetta Ufficiale Della Repubblica Italiana* 04/02/2008, n. 29, S.O. n. 30, 2008. (In Italian)
36. Ohno, K.; Uji, K.; Ueno, A.; Ohtsu, M. Fracture process zone in notched concrete beam under three-point bending by acoustic emission. *Constr. Build. Mater.* **2014**, *67*, 139–145. [CrossRef]
37. Kao, C.S.; Carvalho, F.C.S.; Labuz, J.F. Micromechanisms of fracture from acoustic emission. *Int. J. Rock Mech. Min. Sci.* **2011**, *48*, 666–673. [CrossRef]
38. Aggelis, D.G.; Verbruggen, S.; Tsangouri, E.; Tysmans, T.; Van Hemelrijck, D. Characterization of mechanical performance of concrete beams with external reinforcement by acoustic emission and digital image correlation. *Constr. Build. Mater.* **2013**, *47*, 1037–1045. [CrossRef]
39. Ohtsuka, K.; Date, H. Fracture process zone in concrete tension specimen. *Eng. Fract. Mech.* **2000**, *65*, 111–131. [CrossRef]
40. LUSAS. *User Reference Manual (Version 15.1)*; Finite Element Analysis Ltd.: Kingston upon Thames, UK, 2015.
41. Jagdale, P.M.; Chakrabarti, M.A. Free vibration analysis of cracked beam. *Int. J. Eng. Res. Appl.* **2013**, *3*, 1172–1176.
42. Giannini, O.; Casini, P.; Vestroni, F. Nonlinear harmonic identification of breathing cracks in beams. *Comput. Struct.* **2013**, *129*, 166–177. [CrossRef]
43. Doebling, S.W.; Farrar, C.R.; Prime, M.B.; Shevitz, D.W. *Damage Identification and Health Monitoring of Structural and Mechanical Systems from Changes in their Vibration Characteristics: A Literature Review*; Los Alamos Report LA-13070-MD; Los Alamos National Laboratory: Los Alamos, NM, USA, 1996.
44. Rizos, P.F.; Aspragathos, N.; Dimarogonas, A.D. Identification of crack location and magnitude in a cantilever beam from the vibration modes. *J. Sound. Vib.* **1990**, *138*, 381–388. [CrossRef]
45. Hearn, G.; Testa, R.B. Modal analysis damage detection in structures. *J. Struct. Eng.* **1991**, *117*, 3042–3063. [CrossRef]
46. Pandey, A.K.; Biswas, M.; Samman, M.M. Damage detection in structures using changes in flexibility. *J. Sound. Vib.* **1994**, *169*, 3–17. [CrossRef]
47. Hassiotis, S.; Jeong, G.D. Assessment of structural damage from natural frequency measurements. *Comp. Struct.* **1993**, *49*, 679–691. [CrossRef]
48. Hassiotis, S.; Jeong, G.D. Identification of stiffness reduction using natural frequencies. *J. Eng. Mech.* **1995**, *121*, 1106–1113. [CrossRef]
49. Casas, J.R.; Aparicio, A.C. Structural damage identification from dynamic-test data. *J. Struct. Eng.* **1994**, *120*, 2437–2450. [CrossRef]
50. Silva, J.M.M.; Gomes, A.J.M.A. Crack identification of simple structural elements through the use of natural frequency variations: The inverse problem. In Proceedings of the IMAC XII Conference, Honolulu, HI, USA, 31 January–3 February 1994; pp. 1728–1735.
51. Doyle, J.F. Determining the size and location of transverse cracks in beams. *Exp. Mech.* **1995**, *35*, 272–285. [CrossRef]
52. Khiem, N.T. Damage detection of beam by natural frequencies: General theory and procedure. *Vietnam J. Mech. (VAST)* **2006**, *28*, 120–132. [CrossRef]